Letters

Asymmetric Sampling Disturbance-Based Universal Impedance Measurement Method for Converters

Quansen Rong, Pengfei Hu, *Senior Member, IEEE*, Longyue Wang, Yujing Li, Yanxue Yu, Dong Wang, *Member, IEEE*, and Yu Cao, *Member, IEEE*

***Abstract*—This letter proposes a universal impedance measurement method for grid-connected converter (GCC) where asymmetric disturbances are injected in the sampling process. The goal is to provide a low-cost and easy-implemented impedance measurement technique that does not rely on actual disturbance sources or prior controller knowledge. In this method, only two-phase sampling channels are needed to measure positive- and negative-sequence impedances of GCC at the same time. This method works well with converters employing various control strategies, and its universality is proved by theoretical analysis. The effectiveness of the proposed method is verified by the results of hardware-in-the-loop experiment and the testing of real prototype.**

***Index Terms*—Asymmetric sampling disturbance, converter impedance, grid-connected converter (GCC), harmonic linearization, impedance measurement.**

NOMENCLATURE

V_1	Grid voltage.
v_g	Voltage at the point of common coupling (PCC).
i_o	Output current of GCC.
P^*, Q^*	Reference values of active and reactive power.
D, J	Damping and inertial coefficients of VSG.
ω_0	Angular frequency that is equal to 314 rad/s.
θ	Phase angle produced by PLL or VSG.
A_m	Reference amplitude of ac voltage.
U_d^*, U_q^*	D- and q-axis components of modulation voltage.

I. INTRODUCTION

THE impedance of grid-connected converter (GCC) is applied to analyze the small-signal stability of renewable-energy dominated power systems. Currently, there are three primary methods employed to acquire the impedance of GCC: theoretical model, main-circuit disturbance [1], [2], [3], [4], and controller disturbance [6], [7]. The method based on theoretical models heavily relies on the information regarding controllers provided by manufacturers, which may present practical limitations due to confidentiality reasons. Meanwhile, the main-circuit disturbance-based approach carries with it the burdens of high-cost disturbance sources and complex operations [2], [3]. In an attempt to generate the multioperating-point admittance of converters, artificial neural network has been utilized [4], while the requisite training datasets are sourced from the main-circuit disturbance-based impedance measurement method. Moreover, a variable-operating-point impedance model of the voltage source converter has been obtained in [5], as per impedances obtained by main-circuit disturbance at several preset operating points. To avoid the use of actual disturbance sources, the method that disturbances are directly injected into the controller of GCC, specifically in the modulation signal, has been proposed for measuring the sequence admittance, while only the admittance in the sub/supersynchronous frequency area is implemented [6]. By injecting disturbances along specific control loops within the controller, the admittance of the ac–dc power converter in the full frequency band has been procured [7]. However, the positions and times of disturbance injection are variable for different controllers. Therefore, such methods may encounter limitations and even become impracticable when the controller's information is not available or disturbances cannot be injected within the controller.

To address the limitations of existing impedance measurement methods, this letter proposes a universal

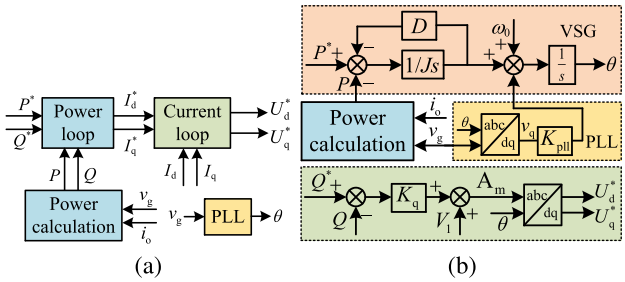

Fig. 1. Block diagrams of (a) PQ and (b) HSC controllers of GCC.

Received 14 June 2024; revised 19 July 2024 and 15 August 2024; accepted 19 August 2024. Date of publication 29 August 2024; date of current version 7 October 2024. *(Corresponding author: Pengfei Hu.)*

Quansen Rong, Pengfei Hu, Longyue Wang, Yujing Li, Yanxue Yu, and Dong Wang are with the College of Electrical Engineering, Zhejiang University, Hangzhou 310000, China (e-mail: 12310093@zju.edu.cn; hpf@zju.edu.cn; 22210020@zju.edu.cn; 12410012@zju.edu.cn; yay@zju.edu.cn; d.wang@zju.edu.cn).

Yu Cao is with the State Grid Zhejiang Electric Power Company, Ltd., Hangzhou Power Supply Company, Hangzhou 310000, China (e-mail: 22110017@zju.edu.cn).

Color versions of one or more figures in this article are available at https://doi.org/10.1109/TPEL.2024.3451403.

Digital Object Identifier 10.1109/TPEL.2024.3451403

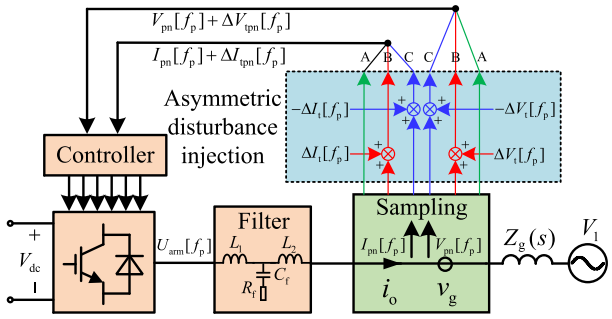

Fig. 2. Asymmetric disturbance injection into sampling values of GCC.

impedance measurement technique for GCC. In this method, asymmetric disturbances are orderly injected into the voltage and current sampling values instead of the controller. We only disturb two-phase sampling values to let the system generate asymmetric disturbance responses, and then obtain positive- and negative-sequence impedances of GCC at the same time. This approach eliminates the need to adjust the positions and times of disturbance injection as per different control strategies, such as grid-following and grid-forming control, irrespective of the presence of additional control loops. Consequently, it enables complete black-box impedance measurement without real disturbance sources. Hardware-in-the-loop (HIL)-based experiment and the testing of real prototype confirm the effectiveness of the proposed method.

II. Universal Impedance Measurement Method for GCC With Various Controllers

This section presents and proves a generalized expression of GCC employing different control strategies. Subsequently, we give the measurement method with asymmetric disturbances injection and impedance calculation. Finally, the analysis of the universality of the proposed method is conducted.

A. Generalized Expression of GCC Controllers Under Disturbance Injection

Two types of control strategies of GCC are given in Fig. 1. The PQ controller, as shown in Fig. 1(a), is composed of the power loop, the current loop, and the phase-locked loop (PLL). As shown in Fig. 1(b), virtual synchronous generator control-based hybrid synchronization control (HSC) [8], [9] is adopted as the grid-forming controller, including active and reactive power loops, and PLL.

The theoretical impedance models of GCC employing grid-following and grid-forming control have been previously established as in [10] and [11]. Utilizing the harmonic linearization modeling theory, it is inferred that the modulation voltages, output by different controllers of GCC, possess a shared characteristic. This finding has led to the innovative presentation of a lemma, substantiated by the following proof.

Lemma 1: For GCC employing any control strategy, the expression of the positive-sequence voltage at the midpoints of three-phase bridge arms, as shown in Fig. 2, $U_{\rm arm}[f_{\rm p}]$, which is generated by modulation voltages through a pulsewidth modulation (PWM) process, is always in the form of (1) after harmonic linearization modeling

$$U_{\rm arm}[f_{\rm p}] = A(s)V_{\rm p}[f_{\rm p}] + B(s)I_{\rm p}[f_{\rm p}] \tag{1}$$

where $s = {\rm j}2\pi f_{\rm p}$, $f_{\rm p}$ is the disturbance frequency, $A(s)$ and $B(s)$ are polynomial fractions in the s-domain related to specific control loops, $V_{\rm p}[f_{\rm p}]$ is the positive-sequence disturbance voltage at PCC in frequency domain, and $I_{\rm p}[f_{\rm p}]$ is the output positive-sequence disturbance current of GCC.

Proof by contradiction is given. First, it is assumed that the voltage at PCC has a small disturbance at $f_{\rm p}$, and $U_{\rm arm}[f_{\rm p}]$ is in the form of (2), as

$$U_{\rm arm}[f_{\rm p}] = A(s)V_{\rm p}[f_{\rm p}] + B(s)I_{\rm p}[f_{\rm p}] + M(s)V_{\rm p}[f_{\rm p}]^m I_{\rm p}[f_{\rm p}]^n \tag{2}$$

where $M(s)$ is a polynomial fraction in the s-domain. In other words, the expression of $U_{\rm arm}[f_{\rm p}]$ includes terms related to $V_{\rm p}[f_{\rm p}]$ and $I_{\rm p}[f_{\rm p}]$.

Then, based on circuit principles, the expression of the main circuit is derived, that is

$$U_{\rm arm}[f_{\rm p}] = P_1(s)V_{\rm p}[f_{\rm p}] + P_2(s)I_{\rm p}[f_{\rm p}] \tag{3}$$

where $P_1(s)$ and $P_2(s)$ are expressions in the s-domain related to the filter. The parameters of the filter are considered to be known through the nameplates of circuit elements. By combining (2) and (3), we obtain the following expression:

$$-\frac{V_{\rm p}[f_{\rm p}]}{I_{\rm p}[f_{\rm p}]} = \frac{P_2(s) - B(s)}{P_1(s) - A(s)} - \frac{M(s)V_{\rm p}[f_{\rm p}]^m I_{\rm p}[f_{\rm p}]^{n-1}}{P_1(s) - A(s)}. \tag{4}$$

As we all know, the positive-sequence impedance of GCC $Z_{\rm p}[f_{\rm p}]$ is defined as the opposite number of the ratio of $V_{\rm p}[f_{\rm p}]$ to $I_{\rm p}[f_{\rm p}]$, where the reference direction of the output current is defined positive when flowing toward the grid. Thus, the left-hand side of the equal sign of (4) is $Z_{\rm p}[f_{\rm p}]$, and it can be seen that $Z_{\rm p}[f_{\rm p}]$ is related to $V_{\rm p}[f_{\rm p}]$ and $I_{\rm p}[f_{\rm p}]$. Namely, if we increase the size of injected disturbances, $V_{\rm p}[f_{\rm p}]$ and $I_{\rm p}[f_{\rm p}]$ will get larger and then $Z_{\rm p}[f_{\rm p}]$ changes. This is explicitly contradictory to the fact that $Z_{\rm p}[f_{\rm p}]$ at $f_{\rm p}$ is a constant complex number under a specific stable operating point. Therefore, the assumption above is not valid and Lemma 1 is proved.

Lemma 1 reveals an essential mechanism that the relational expression between the input values of GCC controllers, $V_{\rm p}[f_{\rm p}]$, $I_{\rm p}[f_{\rm p}]$, and the output voltage, $U_{\rm arm}[f_{\rm p}]$, is consistent with (1), no matter what kind of control strategy is adopted. The same conclusion can also be reached in the negative-sequence coordinate system and the proof process is similar.

B. Impedance Measurement Method Based on Asymmetric Sampling Disturbance

Traditionally, the real impedance of GCC can be obtained by measuring the disturbance responses of the system under main-circuit disturbance. Therefore, by combining (1) and (3), the theoretical positive-sequence impedance model, $Z_{\rm p}(s)$, is derived. The negative-sequence impedance $Z_{\rm n}(s)$ also has the similar expression, as

$$\mathbf{Z_{PN}}(s) = \begin{bmatrix} Z_{\rm p}(s) & \\ & Z_{\rm n}(s) \end{bmatrix} = \begin{bmatrix} \frac{P_2(s)-B(s)}{P_1(s)-A(s)} & \\ & \frac{P_2(s)-D(s)}{P_1(s)-C(s)} \end{bmatrix} \tag{5}$$

where $A(s)$, $B(s)$, $C(s)$, and $D(s)$ are unknown that need to be measured.

The voltage and current disturbances, $\Delta V_{\rm t}[f_{\rm p}]$ and $\Delta I_{\rm t}[f_{\rm p}]$, are injected in the sampling values of phase-B and phase-C, respectively, as shown in Fig. 2, where $V_{\rm dc}$ is the dc voltage, L_1, $C_{\rm f}$, $R_{\rm f}$, and L_2 are parameters of the filter, and $Z_{\rm g}(s)$ is the equivalent grid impedance. The disturbances injected into phase-B and phase-C with a phase difference of 180° to avoid the influence of zero-sequence disturbance component, that is

$$\begin{bmatrix}\Delta X_{\rm tp}\\ \Delta X_{\rm tn}\\ \Delta X_{\rm t0}\end{bmatrix}=\frac{1}{3}\begin{bmatrix}1 & a & a^2\\ 1 & a^2 & a\\ 1 & 1 & 1\end{bmatrix}\begin{bmatrix}0\\ \Delta X_{\rm t}\\ -\Delta X_{\rm t}\end{bmatrix} \tag{6}$$

where $\Delta X_{\rm t}$ is the injected voltage or current disturbance, $a=e^{{\rm j}2\pi/3}$. The subscripts p, n, and 0 represent the positive-, negative-, and zero-sequence components, respectively. Thus, the injected zero-sequence disturbance is zero. Due to the lack of real disturbance sources in the main circuit, $V_{\rm p}[f_{\rm p}]$ is equal to the positive-sequence disturbance voltage of $Z_{\rm g}(s)$, as

$$V_{\rm p}[f_{\rm p}]=Z_{\rm g}(s)I_{\rm p}[f_{\rm p}]. \tag{7}$$

It is interesting that the ratio of $V_{\rm p}[f_{\rm p}]$ to $I_{\rm p}[f_{\rm p}]$ is the grid impedance when disturbances are injected into the sampling values, rather than impedances of GCC under main-circuit disturbance. Substitute (7) into (3), and then the equation of the main circuit under sampling disturbance is obtained

$$U_{\rm arm}[f_{\rm p}]=P_x(s)I_{\rm p}[f_{\rm p}] \tag{8}$$

where $P_x(s)=P_1(s)Z_{\rm g}(s)+P_2(s)$. The value of $Z_{\rm g}(s)$ can be calculated by (7).

According to Lemma 1, when the current disturbance is injected, the disturbance current input into controllers equals the sum of $I_{\rm p}[f_{\rm p}]$ and $\Delta I_{\rm tp}[f_{\rm p}]$. Thus, (1) is changed into

$$U_{\rm arm}[f_{\rm p}]=A(s)V_{\rm p}[f_{\rm p}]+B(s)(I_{\rm p}[f_{\rm p}]+\Delta I_{\rm tp}[f_{\rm p}]). \tag{9}$$

Based on (8) and (9), the expression of GCC under positive-sequence current disturbance is obtained. Furthermore, the negative-sequence components are considered simultaneously

$$\begin{bmatrix}I_{\rm p}[f_{\rm p}]\\ I_{\rm n}[f_{\rm p}]\end{bmatrix}=\mathbf{Y_x}(s)\begin{bmatrix}V_{\rm p}[f_{\rm p}]\\ V_{\rm n}[f_{\rm p}]\end{bmatrix}+\mathbf{G_x}(s)\begin{bmatrix}\Delta I_{\rm tp}[f_{\rm p}]\\ \Delta I_{\rm tn}[f_{\rm p}]\end{bmatrix} \tag{10}$$

where

$$\mathbf{Y_x}(s)=\begin{bmatrix}\frac{A(s)}{P_x(s)-B(s)} & 0\\ 0 & \frac{C(s)}{P_x(s)-D(s)}\end{bmatrix} \tag{11}$$

$$\mathbf{G_x}(s)=\begin{bmatrix}\frac{B(s)}{P_x(s)-B(s)} & 0\\ 0 & \frac{D(s)}{P_x(s)-D(s)}\end{bmatrix}. \tag{12}$$

Similarly, the input disturbance voltage value of the controller is the sum of $V_{\rm p(n)}[f_{\rm p}]$ and $\Delta V_{\rm tp(n)}[f_{\rm p}]$ when the voltage disturbance is injected. Thus, the expression of GCC under voltage disturbance is also derived, that is

$$\begin{bmatrix}I'_{\rm p}[f_{\rm p}]\\ I_{\rm n}{}'[f_{\rm p}]\end{bmatrix}=\mathbf{Y_x}(s)\begin{bmatrix}V'_{\rm p}[f_{\rm p}]+\Delta V_{\rm tp}[f_{\rm p}]\\ V_{\rm n}{}'[f_{\rm p}]+\Delta V_{\rm tn}[f_{\rm p}]\end{bmatrix}. \tag{13}$$

By solving (10) and (13), $\mathbf{Y_x}(s)$ and $\mathbf{G_x}(s)$ at $f_{\rm p}$ are calculated. Then, another part of the impedance of GCC is defined as $\mathbf{Y_0}(s)$, that is

$$\mathbf{Y_0}(s)=\begin{bmatrix}\frac{P_1(s)}{P_x(s)-B(s)} & 0\\ 0 & \frac{P_1(s)}{P_x(s)-D(s)}\end{bmatrix}. \tag{14}$$

Through some derivations, $\mathbf{Y_0}(s)$ at $f_{\rm p}$ is acquired by the calculated value of matrix $\mathbf{G_x}(s)$

$$\mathbf{Y_0}(s)=\frac{P_1(s)}{P_x(s)}[\mathbf{I}+\mathbf{G_x}(s)]. \tag{15}$$

Therefore, $\mathbf{Z_{PN}}(s)$ is finally achieved by

$$\mathbf{Z_{PN}}(s)=\mathbf{K}(s)[\mathbf{Y_0}(s)-\mathbf{Y_x}(s)]^{-1} \tag{16}$$

where the expression of matrix $\mathbf{K}(s)$ is

$$\mathbf{K}(s)=\frac{P_2(s)}{P_1(s)}\mathbf{Y_0}(s)-\mathbf{G_x}(s). \tag{17}$$

$\mathbf{K}(s)$ describes the effect of the grid impedance. When the grid is ideal such that $Z_{\rm g}(s)=0$, it can be seen that $P_x(s)=P_2(s)$ by (8). Thus, $\mathbf{K}(s)=\mathbf{I}$, according to (12), (14), and (17). Then, $\mathbf{Z_{PN}}(s)$ is correctly calculated by (16). For the coupling impedances in the off-diagonal positions, they could be measured and calculated as (13). The difference is that the current responses at the coupling frequency are needed to be extracted, and only once voltage sampling disturbance is required.

C. Discussion for the Universality of the Proposed Method

In practice, the manufacturers generally do not disclose the internal information of their control loops, which renders the controller of GCC a black box. Consequently, impedance measurement operators will face significant challenges in introducing disturbances inside the GCC controller, barring an instance of obtaining explicit permission and cooperation from manufacturers. In addition, a variety of existing control strategies are combined with various additional control loops, such as virtual impedance loop, voltage feedforward loop, and current feedback loop, which makes the controllers diverse. Therefore, it inevitably becomes an arduous task to adjust the positions and times of disturbance injection according to the specific controllers of GCC as [7].

The proposed method is universal for GCC with various controllers and only the parameters of the filter are needed, making it possible to realize low-cost and black-box impedance measurement. In this approach, the effect of the grid impedance is described as (17) so that it is applicable under different grid strength. No matter which control strategy is adopted, the output positive-sequence voltage of the GCC controller, $U_{\rm arm}[f_{\rm p}]$, is always in the form of (1). The things that change are $A(s)$ and $B(s)$ determined by the specific controller of GCC. It still holds for the negative-sequence impedance. Thus, the impedance of GCC will be achieved once $A(s)$, $B(s)$, $C(s)$, and $D(s)$ have been obtained. Based on (10) and (13), $\mathbf{Y_x}(s)$ and $\mathbf{G_x}(s)$ can be calculated. $B(s)$ is then obtained since it is the only unknown variable in (12). Substitute the value of $B(s)$ into (11),

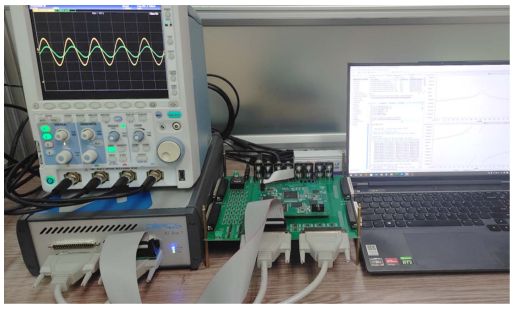

Fig. 3. RT-BOX-based HIL experiment platform.

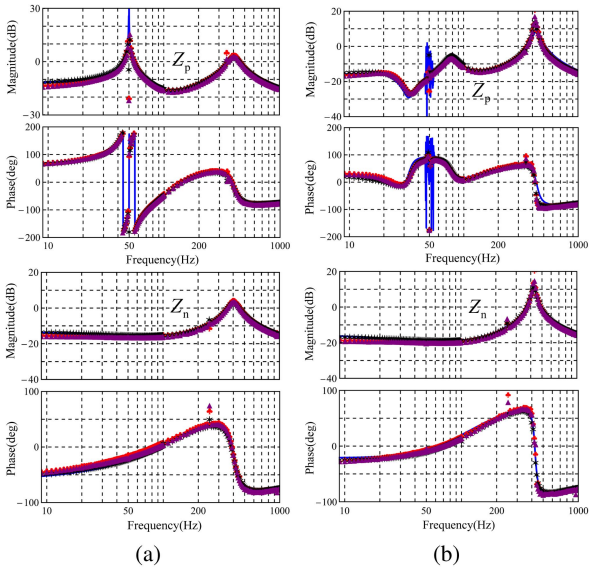

Fig. 4. Impedance measurement results of GCC with (a) PQ and (b) HSC controllers. Solid lines: theoretical models; Black dots: results by main-circuit disturbance; Red and purple dots: results by asymmetric sampling disturbance with L_g equals 0.05 and 0.15 mH, respectively.

$A(s)$ is finally calculated. The above calculation process is also applicable to $C(s)$ and $D(s)$.

Compared to the conventional main-circuit disturbance-based measurement method, the expensive large-capacity disturbance sources are not needed. The asymmetric disturbances are injected into the sampling values of two phases, which can be implemented by digital chips with lower measurement cost and more simple operations. This method can be utilized for small-signal stability analysis of renewable-energy systems by its potential of real-time impedance measurement.

III. Experimental Verification of the Proposed Impedance Measurement Method

A. HIL-Based Experimental Verification

The effectiveness of the proposed asymmetric sampling disturbance-based impedance measurement method for GCC is verified through the HIL experiment as follows. The HIL experiment platform is shown in Fig. 3, including RT-BOX, TMS320F28335, and a host computer.

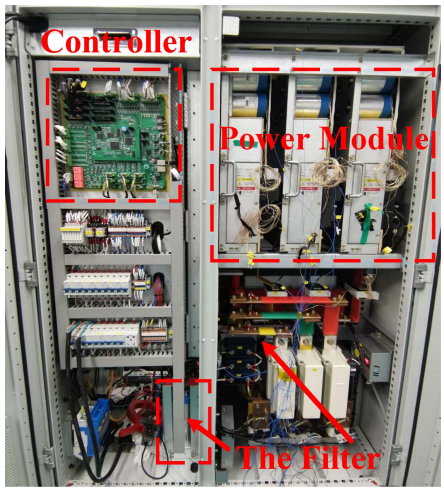

Fig. 5. Real prototype based on two-level power converter.

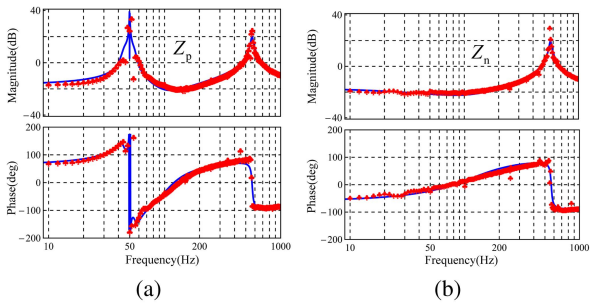

Fig. 6. Positive- and negative-sequence impedance measurement results of the prototype testing. Solid lines: theoretical models; Red dots: results by asymmetric sampling disturbance.

TABLE I
Parameters of the Main Circuit

Parameter	Value	Parameter	Value
V_1	311 V	L_2	0 mH
V_{dc}	800 V	C_f	990 μF
L_1	0.16 mH	R_f	0.033 Ω

TABLE II
Parameters of the Controllers

PQ Controller		HSC Controller	
P^*, Q^*	250 kW, 0 kVar	P^*, Q^*	250 kW, 0 kVar
PQ: k_p, k_i	0.2, 40	J, D	10, 160
I: k_p, k_i	0.1, 50	K_{pll}	0.067
PLL: k_p, k_i	0.28, 12	K_q	0.4

Two control strategies, as shown in Fig. 1, are employed to test the performance and universality of the proposed method. The parameters are listed in Tables I and II, where L_g is the equivalent inductance of the grid and it is set to possess two values, respectively, 0.05 and 0.15 mH, to validate the accuracy of the proposed method under different grid conditions, and k_p and k_i are the proportional and integral coefficients of different control loops, respectively. PQ, I and PLL represent the power

TABLE III
PARAMETERS OF THE POWER CONVERTER

Parameter	Value	Parameter	Value
V_1	326.6 V	L_2	0 mH
V_{dc}	750 V	PQ: k_p, k_i	0.2, 10
C_f	628 μF	I: k_p, k_i	0.1, 50
R_f	0.143 $m\Omega$	PLL: k_p, k_i	0.28, 12
L_1	0.125 mH	P^*, Q^*	10 kW, 0 kVar

loop, the current loop, and the PLL, respectively. The switching frequency of PWM is 5 kHz.

The sine wave at a certain frequency is set as the injected disturbance signal. Two measurement processes are included that disturbance signals are superimposed with the sampling values of the output current of GCC, and then the voltage at PCC, as shown in Fig. 2. After each disturbance injection, waveforms of the voltage at PCC, the output current of GCC, and corresponding injected disturbances are recorded. The sampling frequency of the waveforms is 10 kHz. It is worth noting that the amplitudes of injected disturbances are set to be around 5% of the steady-state voltage and current values to avoid huge disturbance responses of the system.

Given the wide-ranging applicability of the proposed method, the procedures of impedance measurement remain unchanged when the controller of GCC changes. Based on the analysis above, the impedance measurement results are presented in Fig. 4, where the blue lines are impedance theoretical models, the black dots show the results of main-circuit disturbance-based method, and the red and purple dots represent those of the proposed method under different grid conditions. The impedance measurement results of the proposed method are generally the same as those of main-circuit disturbance-based method and theoretical models, although there is a slight measurement error in the low-frequency range around 10–20 Hz. Therefore, the universality and effectiveness of the proposed method are verified by HIL experimental results.

B. Experimental Testing of Real Prototype

In order to verify the validity of the proposed method in practice, a real prototype based on the two-level power converter with FF600R12ME4 IGBT is established, as in Fig. 5, where the converter is connected to the grid through a SGB-60KVA transformer. The ac-side impedance of the converter is to be measured and its dc-side voltage is generated by an uncontrolled rectifier circuit. In Fig. 5, TMS320F28335 DSP is adopted as the controller, which is used to inject sampling disturbances and realize real-time calculation of the impedance of the converter. The converter adopts the control strategy, as shown in Fig. 1(a), and the parameters are listed in Table III. The switching frequency of PWM is 2.7 kHz and the sampling frequency is 10 kHz.

Disturbances are injected into the current and voltage sampling values in turn, and the output voltage and current waveforms of the converter are recorded. The output disturbance responses of the converter at the disturbance frequency and the corresponding injected disturbances are extracted to calculate the converter's positive- and negative-sequence impedances. The impedance measurement results of the proposed method are shown in Fig. 6. Compared with the theoretical impedance models, the trend and accuracy of the results of the proposed method are satisfactory and can meet the requirements of practical engineering.

IV. CONCLUSION

In this letter, we propose a novel and easy-implemented black-box impedance measurement method. This approach is universally applicable to GCC with various control loops, achieved by injecting asymmetric disturbances into two-phase sampling values. Notably, there is no need to be informed of the internal information of the controller in advance, and the controller is not mandatory for internal disturbance injection. It indicates that the functions and applications of this proposed method are almost the same as those of the main-circuit disturbance-based impedance measurement method, while the cost of real disturbance sources is eliminated and operations are simplified. The HIL experiment and prototype testing verify the effectiveness of the proposed method.

ACKNOWLEDGMENT

The authors would like to thank engineers Huasen Ying, Ziwen Xu, Zhenjun Gao, and Azhen Zhou for their efforts in the real prototype experiments.

REFERENCES

[1] J. Pedra, L. Sainz, and L. Monjo, "Review and improvements to the measurements of the VSC impedance transfer matrix," *IEEE Trans. Power Del.*, vol. 39, no. 2, pp. 1283–1298, Apr. 2024.
[2] J. Ma, W. Wang, S. Wang, T. Liu, and J. Zhao, "Bidirectional power balance control of serial voltage injection converter for impedance measurement of grid-connected inverter," *IEEE Trans. Power Electron.*, vol. 38, no. 6, pp. 7069–7078, Jun. 2023.
[3] H. Gong, X. Wang, and D. Yang, "DQ-frame impedance measurement of three-phase converters using time-domain MIMO parametric identification," *IEEE Trans. Power Electron.*, vol. 36, no. 2, pp. 2131–2142, Feb. 2021.
[4] M. Zhang, X. Wang, D. Yang, and M. G. Christensen, "Artificial neural network based identification of multi-operating-point impedance model," *IEEE Trans. Power Electron.*, vol. 36, no. 2, pp. 1231–1235, Feb. 2021.
[5] W. Liu, X. Xie, J. Shair, and J. Zhang, "Stability region analysis of grid-tied voltage sourced converters using variable operating point impedance model," *IEEE Trans. Power Syst.*, vol. 38, no. 2, pp. 1125–1137, Mar. 2023.
[6] Z. Xie, W. Wu, Y. Chen, S. Cao, and Y. Xu, "Sequence-admittance measurement method of grid-connected inverter with its control system disturbance," *IEEE Trans. Ind. Electron.*, vol. 70, no. 8, pp. 8598–8602, Aug. 2023.
[7] C. Sun, X. Ding, L. Zhang, H. Guo, and J. Chen, "Self-measurement of the admittance matrix of AC-DC power converter by internal harmonic injection," *IEEE Trans. Ind. Electron.*, vol. 71, no. 2, pp. 1503–1513, Feb. 2024.
[8] T. Liu and X. Wang, "Physical insight into hybrid-synchronization-controlled grid-forming inverters under large disturbances," *IEEE Trans. Power Electron.*, vol. 37, no. 10, pp. 11475–11480, Oct. 2022.
[9] P. Hu, W. Jiang, Y. Yu, D. Jiang, and M. Guerrero, "Transient stability improvement of grid-forming voltage source converters considering current limitation," *Sustain. Energy Technol. Assessments*, vol. 54, 2022, Art. no. 102839.
[10] M. Cespedes and J. Sun, "Impedance modeling and analysis of grid-connected voltage-source converters," *IEEE Trans. Power Electron.*, vol. 29, no. 3, pp. 1254–1261, Mar. 2014.
[11] W. Wu et al., "Sequence impedance modeling and stability comparative analysis of voltage-controlled VSGs and current-controlled VSGs," *IEEE Trans. Ind. Electron.*, vol. 66, no. 8, pp. 6460–6472, Aug. 2019.